Electronic Supplementary Information

Mimicking NADPH Oxidase and Lipoxygenase by Biodegradable Single-site Catalyst via Cascade Reaction to Trigger Tumor-selective Ferroptosis

Xiyang Ge,[a] Yiyan Yin,[a] Xiaoni Wang,[a] Xiang Li,[a,b] Jin Ouyang,[c] Na Na[*a]*

[a] Key Laboratory of Radiopharmaceuticals, College of Chemistry, Beijing Normal University, Beijing 100875, China.

[b] State Key Laboratory for Quality Ensurance and Sustainable Use of Dao-di Herbs, National Resource Center for Chinese Materia Medica, China Academy of Chinese Medical Sciences, Beijing 100700, China

[c] Department of Chemistry, College of Arts and Sciences, Beijing Normal University, Zhuhai, 519087, China

* Corresponding author E-mail: nana@bnu.edu.cn.

1. Experimental Section

1.1 Materials and Instruments

$H_3PW_{12}O_{40}$ (PW_{12}), $FeCl_3 \cdot 6H_2O$, H_2BDC, and NADPH were obtained from Aladdin Biochemical Technology Co., Ltd. (Shanghai, China). Iron oxide nanoparticle (Fe_3O_4), glutathione reduced (GSH), 5,5' -dithiobis-2-(nitrobenzoicacid) (DTNB), 10-Acetyl-3,7-dihydroxyphenoxazine (ADHP) and H_2O_2 (30%) were purchased from Innochem (Beijing, China). Horseradish peroxidase (HPR), Dulbecco's modified Eagle's medium (DMEM), trypsin, phosphate-buffered saline (pH 7.4 and pH 5.5) and fetal calf serum (FBS) were acquired from Sigma-Aldrich. Dihydroethidium (DHE), 2',7'-dichloro fluorescein diacetate (DCFH-DA), 3-[4,5-dimethylthiazolyl-2-]-2,5-diphenyltetraolium bromide (MTT), JC-1, propidium iodide (PI) and Calcein AM detection kit were purchased from Solarbio Science & Technology. GSH assay kit and WST-8 ($NADP^+$/NADPH) assay kit were purchased from Beyotime (China). Human Coenzyme Q_{10} (CoQ_{10}) ELISA Kit and Human BH_4 ELISA Kit were purchased from Shanghai Hengyuan Biotechnology (China). Methanol of HPLC grade was purchased from Fisher Chemical (CA, USA). Ultrapure water (Mill-Q, Millipore, 18.2 MΩ) was used in all experiments. All chemicals were used as received without further purification.

Transmission electron microscopy (TEM) measurements were carried out on a Talos F200S transmission electron microscope (Thermo Fisher Scientific). High-angle annular dark-field scanning transmission electron microscopy (HAADF-STEM) characterization was conducted on an FEI Themis Z. Powder X-ray diffraction patterns were recorded by Shimadzu XRD-7000 with Cu Kα radiation (λ = 1.5418 Å). Ultraviolet-visible (UV-vis) spectra were acquired using a Shimadzu UV-2600 spectrophotometer (Shimadzu, Japan). The fluorescence spectra were recorded on an FS5 fluorescence spectrometer (Edinburgh, UK). Fourier Transform infrared spectroscopy (FTIR) spectra were obtained on a Thermo Scientific Nicolet iS20. The dynamic light scattering (DLS) and zeta potential data were conducted using the Nano-ZS Zetasizer ZEN3600 (Malvern, UK). The loading efficiency was performed by Agilent 1260 high-performance liquid chromatography (HPLC) with mobile phase (methanol/ phosphate buffer v/v 7:3, pH=4.5). MS analysis was performed using an LTQ XL linear ion trap mass spectrometer (Thermo Fisher Scientific). Online monitoring of the degradation of MIL-101@PW_{12} and the formation of Fe-PW_{11} was carried out using a homemade ionization source. The HRMS experiments for the liquid phase were detected by a G2-XS QTof mass spectrometer (Waters). The cell viability was measured by thiazolyl blue tetrazolium

bromide (MTT) using a microplate reader at 490 nm on a microplate reader (BioTek, USA). Confocal fluorescence imaging of cells was performed on a Nikon A1R-si laser confocal laser scanning microscope (CLSM) (Nikon, Japan).

1.2 The Synthesis of MIL-101

The MIL-101 NPs were prepared by solvothermal method according to previous reports.[14] Briefly, 5 mmol of $FeCl_3 \cdot 6H_2O$ and 2.5 mmol of H_2BDC were dissolved in 30 mL of N, N-dimethylformamide (DMF), packaged in a stainless steel autoclave lined, and kept at 120 °C in an oven for 12 h. After naturally cooling down to room temperature, the precipitates were obtained by centrifugation at 12000 rpm for 10 min, and washed three times with deionized water and ethanol, respectively.

1.3 The Synthesis of MIL-101@PW_{12}

The MIL-101 NPs (5 mg) and PW_{12} (2 mg) were dispersed in 20 mL of methanol by continuous stirring at room temperature for 4 h. Then the obtained MIL-101@PW_{12} NPs were collected by centrifugation at 12000 rpm for 5 min, and washed with methanol and deionized water several times.

1.4 The Synthesis of A-MIL-101@PW_{12}

1.5 mL MIL-101@PW_{12} (1 mg/mL) was mixed with 30 μL AS1411 aptamer (10 μM) for string 24 h in the dark. The obtained A-MIL-101@PW_{12} was washed with deionized water several times. The loading efficiency of PW_{12} in MIL-101 was measured by the HPLC and calculated according to the standard calibration curve.

1.5 Stability of A-MIL-101@PW_{12}

The prepared A-MIL-101@PW_{12} was added into deionized water and stirred continuously for 4 h until evenly dispersed, and the supernatant solution was tested by electrospray ionization (ESI-MS). In addition, the A-MIL-101@PW_{12} was dispersed in water, PBS and DMEM culture medium and incubated at 37 ℃ for 0, 12, 24, and 48 hours. The stability of the A-MIL-101@PW12 was evaluated using hydrodynamic size distributions (DLS) analysis.

1.6 The transformation of PW_{12} to PW_{11}

10 ug/mL PW_{12} was added into ammonium acetate buffer with pH 5.5 and the solution was detected by MS. The Fe^{2+} was added to the PW_{12} solution at pH 5.5 and the solution was also detected by MS.

1.7 Degradation of A-MIL-101@PW_{12}

A-MIL-101@PW_{12} (5 mg) was dispersed in 10 mL GSH (10 mM) with string 4 h, and the mixture solution was detected by ESI-MS. For ICP-OES, MIL-101@PW_{12} (5 mg) was dispersed in 10 mL phosphate-buffered saline (pH=5.5) with different concentrations of GSH solution (1 mM or 10 mM) under magnetic stirring. At varied time points, the liquid (200 μL) was obtained from the mixed solution and then centrifuged. The supernatant was added to 4 mL of deionized water and measured by ICP-OES to determine the concentrations of released Fe and W elements. Furthermore, the extracted ion chromatograms (EICs) of the formation of Fe-PW_{11} were achieved by a homemade ionization source (EESI-MS). Briefly, 2 mg/mL MIL-101@PW_{12} was dispersed in 10 mM ammonium acetate buffer solution (pH=5.5) with 5 mM GSH solution, and the solutions were detected in real-time.

1.8 The EPR measurement

EPR was carried out to detect the spin state of Fe of in situ synthesized Fe(II)-PW_{11} and Fe(III)-PW_{11}-O_2^- intermediate through freeze-drying to powder. EPR was carried out to detect $NADP^{\bullet}$ by mixing 1 mg/mL Fe(II)-PW_{11} and 1 mM NADPH in the solution containing 5-(2,2-dimethyl- 1,3-propoxycyclo-phosphoryl)-5-methyl-1-pyrroline N-oxide (CYPMPO, 100 mM). EPR was carried out to detect LA radicals by mixing 1 mg/mL Fe(II)-PW_{11} with 1 mM NADPH and 1 mM LA in the solution containing 5-tert-butoxycarbonyl (BMPO,100 mM).

1.9 $NADP^+$ detection

1 mg/mL Fe-PW_{11} was mixed with 1 mM NADPH and the $NADP^+$ was detected by ESI-MS with the solution of the ratio of methanol to water is 1:1.

1.10 H_2O_2 detection

10-Acetyl-3,7-dihydroxyphenoxazine (ADHP) is a highly sensitive and stable peroxidase substrate that can be used to selectively detect H_2O_2. In the horseradish peroxidase (HRP) system, colorless and non-fluorescent ADHP reacts with H_2O_2 in a 1:1 semiquantitative ratio to form Resorufin. The mixture was recorded by the UV-visible absorption spectrum at 570 nm. 1 mg/mL Fe(II)-PW_{11}, 1 mM NADPH, and 0.1 ug/mL Horseradish Peroxidase (HPR) were mixed in the PBS containing 1 mM ADPH to detect the generation of H_2O_2.

1.11 PUFA and PUFA-PLs detection

The online monitoring of the catalytical reaction was carried out through EESI-MS. 1 mg/mL Fe(II)-PW_{11}, 1 mM linoleic acid (LA)/oleic acid (OA)/lecithin (PC)/cuorin (CL) and 1 mM NADPH solution

were mixed. The mass spectrum signal of the reaction mixture was measured every 5 minutes. The reaction intermediates absorbed on the Fe(II)-PW_{11} were detected by ESI-MS with the solution of the ratio of methanol to water 1:1 in the Zoom model.

1.12 Electrochemical measurement

The standard three-electrode cell, consisting of glassy carbon as a working electrode, was used for cyclic voltammetry (CV). A Silver/silver chloride (Ag/AgCl) electrode was used as a reference electrode and the platinum sheet electrode was used as an auxiliary electrode. CV scanning was conducted with a voltage range between -1.00 and 1.50 V (scan rate: 100 mV/s). In order to compare the CV curve of Fe(II)-PW_{11} with N_2 or O_2, 1 mM NADPH was added to the Fe(II)-PW_{11} solution with N_2 and O_2 to achieve the electron transfer process between Fe-PW_{11} and NADPH under N_2 and O_2 conditions.

1.13 Cell Culture

Human cervical adenocarcinoma epithelial cells (HeLa cells) and Human Umbilical Vein Endothelial Cells (HUVECs) were cultured with regular growth media consisting of high glucose DMEM. The cell growth media were supplemented with 10% FBS, 100 U/mL penicillin, and 100 mg/mL streptomycin and cultured at 37 °C in a 5% CO_2 humidified environment. The media was changed every two days and the cells were digested by trypsin, which was then re-suspended in a fresh medium before plating.

1.14 The detection of in situ synthesis of Fe(II)-PW_{11} in cancer cells

HeLa cells were seeded in the petri dish with A-MIL-101@PW_{12} addition for 12 h. Subsequently, cells were collected and lysed, and the supernatant was detected by ES-MS with the solution of the ratio of methanol to water of 1:1.

1.15 Intracellular GSH and NADPH levels

To determine intracellular GSH and NADPH levels of HeLa cells, cells were seeded in 6-well plates (2×10^5 cells per well) and treated with different groups. Subsequently, cells were collected and the intracellular GSH and NADPH level for HeLa cells was tested by using the GSH and NADPH Assay Kit.

1.16 Intracellular CoQ_{10} and BH_4 levels

HeLa cells were seeded in 6-well plates (2×10^5 cells per well) and treated with different groups. Subsequently, cells were collected and the intracellular CoQ_{10} and BH_4 level for HeLa cells was tested by using the Human Coenzyme Q_{10} (CoQ_{10}) ELISA Kit and Human BH_4 ELISA Kit.

1.17 Cell imaging

For the live/dead cell staining assay, HeLa cells and HUVECs were planted in the dish and treated with different groups in 4 mL of neutral DMEM containing 10% FBS. After that, the DMEM was added to different groups. After another 12 h, the cells were washed three times with PBS, followed by staining with Calcein AM (10 μM) and PI (20 μM). After 20 minutes of incubation, the medium was removed and the cells were washed three times with PBS. The fluorescence imaging of cells was analyzed by fluorescence microscopy.

1.18 Cell viability test

To investigate the toxicity of A-MIL-101@PW_{12}, HeLa cells and HUVEC were planted in 96-well plates and treated with different groups. Briefly, HeLa cells or HUVECs (~5000 cells) were pre-incubated at a density of 5000 cells per well for 12 h. Then, the cells were incubated in different groups for 12 h. Then, the solution in the wells was removed and 100 μL of 3-(4,5-dimethyl-2-thiazolyl)-2,5-diphenyl-2-H-tetrazolium bromide (MTT, 0.5 mg/mL in PBS) solution was added to each plate. Then the solution in each well was carefully removed and replaced by 100 μL DMSO to dissolve the formazan. The Cell cytotoxicity was measured by the absorbance at 570 nm.

1.19 Western blotting

HeLa cells were placed in 6-well plates (2×10^5 cells per well). Then PBS, Fe(II)-PW_{11} and A-MIL-101@PW_{12} were incubated with cells for 24 hours. The culture medium was added to terminate after digesting. The samples were centrifuged at 845 g for 10 minutes before discarding the supernatant. 500 μL SDS lysis buffer was added to each tube to extract the total protein and then the mixture was heated at 100 ℃ for 10 minutes. The concentration of protein was determined with the BCA Protein Quantification Kit. The proteins were separated on 10% SDS-polyacrylamide gel electrophoresis with SDS loading buffer and then electro-transferred onto a PVDF transfer membrane with WB Transfer Buffer at 220 mA for 2.5 h. The membranes were blocked with 5% nonfat dry milk in TBST buffer for 1 h at room temperature. The membranes were incubated overnight at 4 °C with corresponding anti-GPX4/anti-FSP1/anti-DHFR (1:1000) antibodies in TBST. After three times of successive washes with TBST for 10 min, the membranes were incubated with

secondary antibodies in TBST for 1 h at room temperature. After three successive washes with TBST for 10 min, protein expressions were determined using a Super Signal chemiluminescence system (ECL) and photographed by an automatic chemiluminescence image processing system (Tannon-4600SF).

1.20 In vivo antitumor performance

The tumor (HeLa) bearing Balb/c nu female mouse (6 weeks) model was built by subcutaneous injection of HeLa cells (2×10^7 mL^{-1}, 100 μL) into the axilla of each mouse. Tumor (HeLa) bearing mice (tumor volume: ~100 mm^3) were randomly divided into five groups (3 mice in each group): saline group (control), MIL-101 group (I), Fe(II)-PW_{11} group (II), MIL-101@PW_{12} group (III) and A-MIL-101@PW_{12} group (IV). Then, 1.20 mg/kg of nanomedicine was injected into mice in each administration group by intravenous injections. The tumor size was measured every two days and calculated by: V = 1/2 (tumor length) × (tumor width)^2. After two weeks, tumors and main organs were collected from the killed mice for further analysis.

1.21 Hemolysis assay

Red blood cells (RBCs) were collected and purified to be resuspended in 5 mL saline. 0.2 mL of RBCs was incubated with 0.8 mL AMIL-101@PW_{12} in saline with different concentrations for 30 min at 37°C, respectively. AMIL-101@PW_{12} (100 μg/mL, 200 μg/mL, 400 μg/mL and 800 μg/mL), saline (negative control) and Triton X-100 (positive control) were incubated with RBCs, respectively. After centrifugation (3000 g, 10 min), the supernatant was obtained to detect the absorbance at 570 nm. The hemolysis (%) was calculated by the following equation:

$$Hemolysis = \frac{sample - negative}{positive - negative} \times 100\% \quad (1)$$

where sample is the absorbance of supernatant after incubation of blood and materials, negative and positive are the absorbance of supernatant after incubation of saline, respectively.

1.22 Histological analysis

All mice of different groups were sacrificed on the 15th day, and major organs and tumors were separated and made into slices for H&E and Ki67 staining. Major organs were collected and fixed in 4% paraformaldehyde, which was then embedded in paraffin to obtain the slices at the thickness of 5 μm. The tissue slices were stained with H&E and Ki67 and then imaged by optical microscopy and assessed by 3 independent pathologists.

1.23 Serum biochemistry measurement.

The samples of eyeball blood were collected from mice of different groups. Serum was obtained by centrifuging (4 ℃) the blood samples at 845 g for 10 minutes, and detected by a biochemical analyzer (BK400, BIOBASE, China). The detection indicators included total protein (TP), albumin (ALB), alanine transferase (ALT), alkaline phosphatase (ALP), aspartate aminotransferase (AST), uric acid (UA), creatinine (CREA), creatine kinase (CK), creatine kinase MB (CK-MB), triglyceride (TG), lactate dehydrogenase (LDH).

1.24 Computational Methods

All the calculations were solved utilizing density functional theory in the Gaussian 09 program.[1] All the molecules were optimized by the hybrid M06L. The Lanl2TZ basis function was used for the Mn and 6-311G** was used for the other atoms (P, W, H and O). All the structure optimization and the energy calculations were performed using a continuum description of solvent based on an SCRF method and the solvent was defined as a water solution. The result of the computation was further processed via the Multiwfn software package (v 3.8).[2] The ESP potential figure of PW_{11} and Fe(II)-PW_{11} was carried out using the VMD 1.9.4 software.[3]

1.25 Statistical analysis

The results were presented as mean values of replicate experiments or replicate samples in one representative experiment, as indicated in the figure legends. Statistical analysis was performed using GraphPad Prism and $p < 0.05$ was considered statistically significant. Dose-response curves were fitted using a four-parameter logistic (4PL) nonlinear regression model in GraphPad Prism version 9.5.0 for Win (GraphPad Software, Boston, USA, www.graphpad.com). The LD_{50} values with 95% confidence intervals (CI) were derived from the curve fit.

2 Supporting Figures

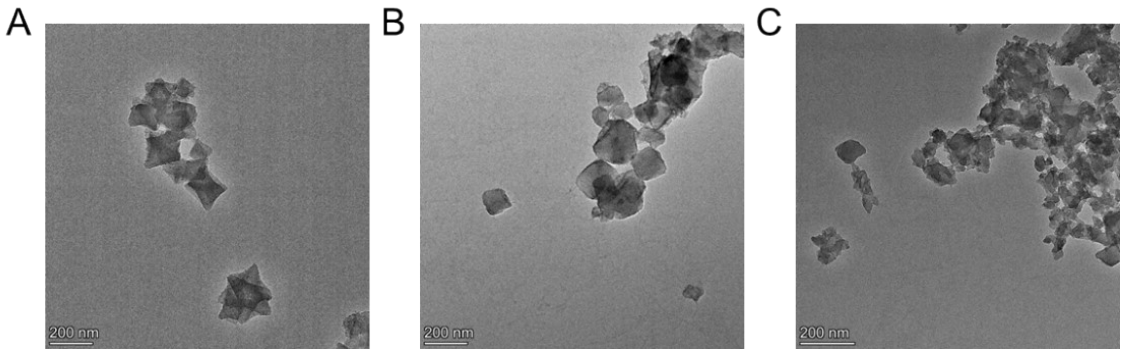

Fig.S1 TEM images of (A) MIL-101, (B) MIL-101@PW_{12} and (C) A-MIL-101@PW_{12}.

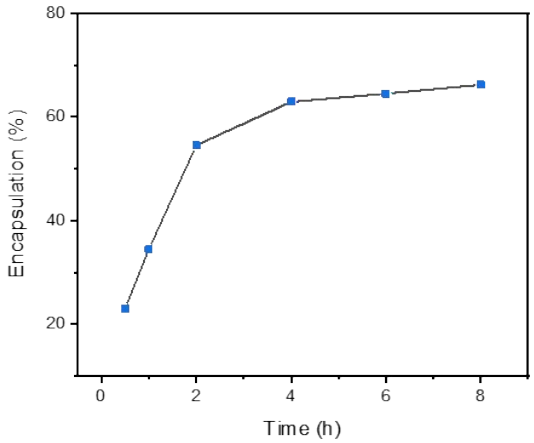

Fig. S2 The encapsulation of PW_{12} at different times.

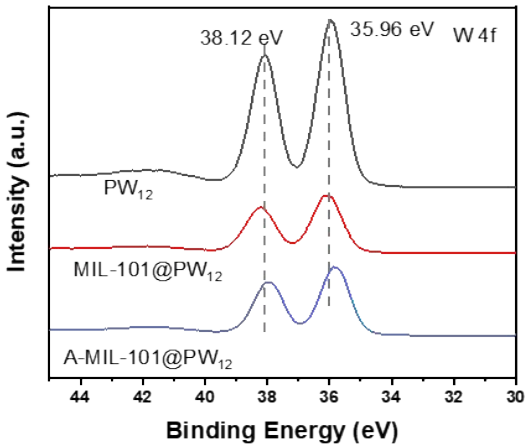

Fig. S3 W 4f XPS of PW_{12}, MIL-101@PW_{12} and A-MIL-101@PW_{12}.

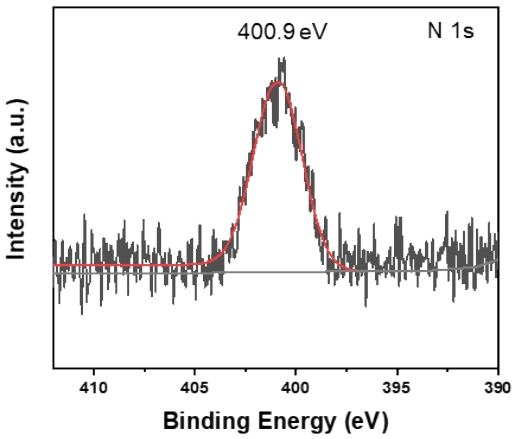

Fig. S4 N 2s XPS of A-MIL-101@PW_{12}.

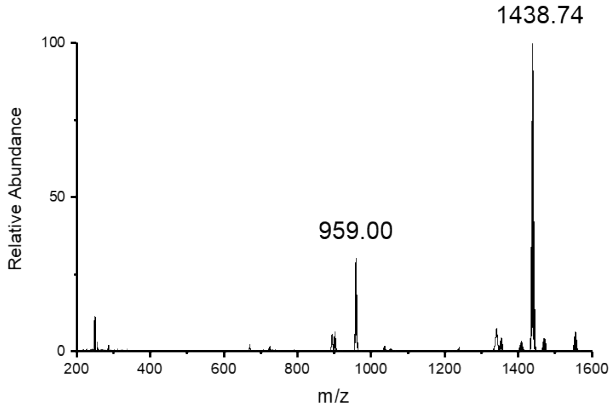

Fig. S5 MS signal of PW_{12}.

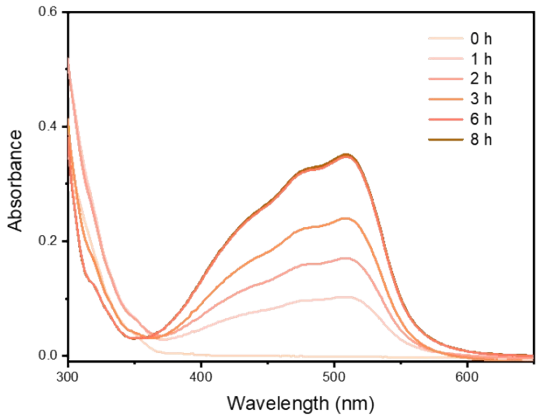

Fig. S6 The UV-vis spectra of MIL-101@PW_{12} for Fe^{2+} detection with 10 mM GSH concentrations at different times using chelated 1,10-phenanthroline as indicator.

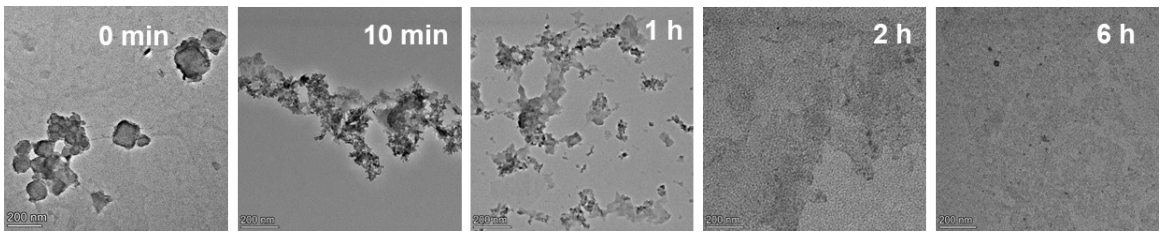

Fig. S7 The TEM images of degradation of A-MIL-101@PW_{12} in 10 mM GSH solutions at different times.

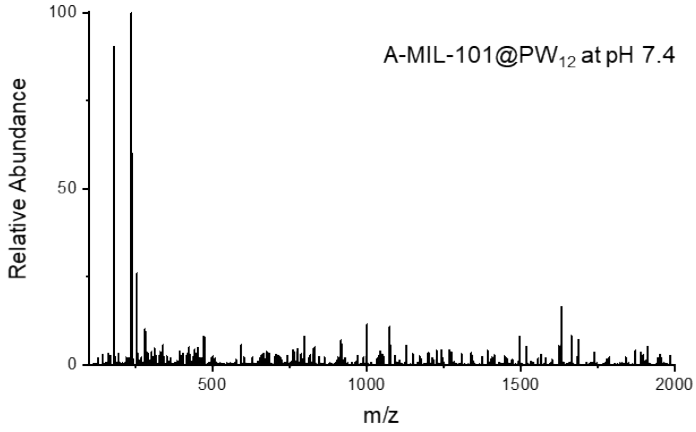

Fig. S8 MS spectra of A-MIL-101@PW_{12} at PBS solution with pH 7.4.

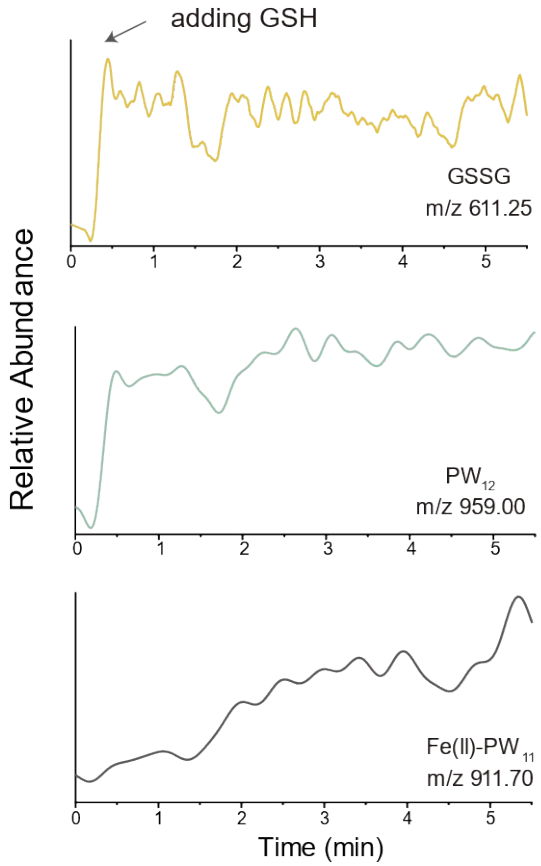

Fig. S9 Online monitoring of the degradation of A-MIL-101@PW_{12} treated with 10 mM GSH treatment at pH 5.5

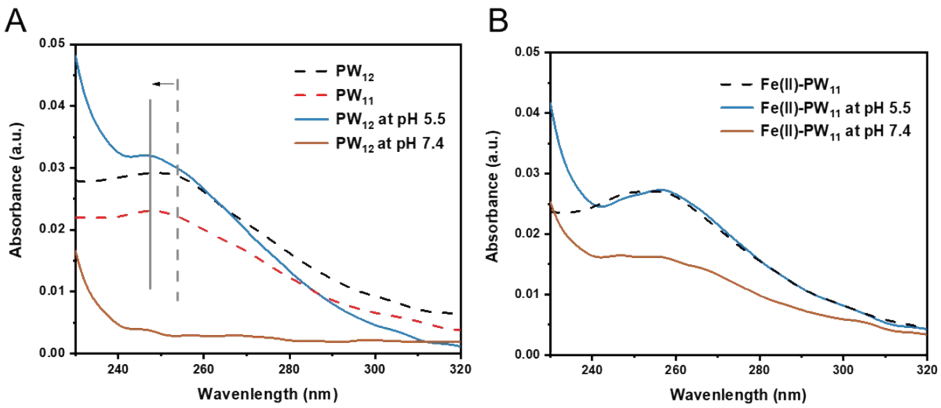

Fig. S10 The UV-vis spectra of PW_{12} and Fe(II)-PW_{11} in different pH solutions.

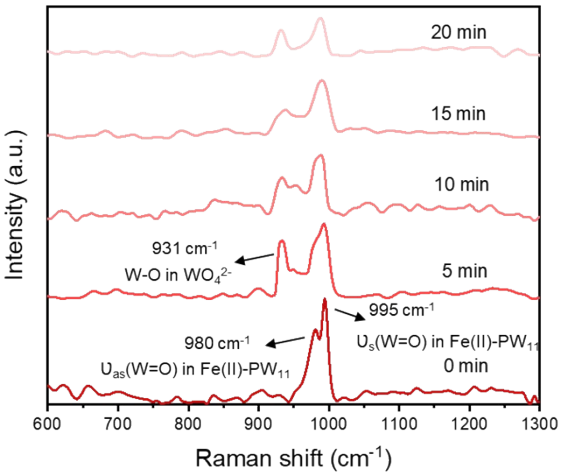

Fig. S11 The in-situ Raman spectra of Fe(II)-PW_{11} under neutral conditions.

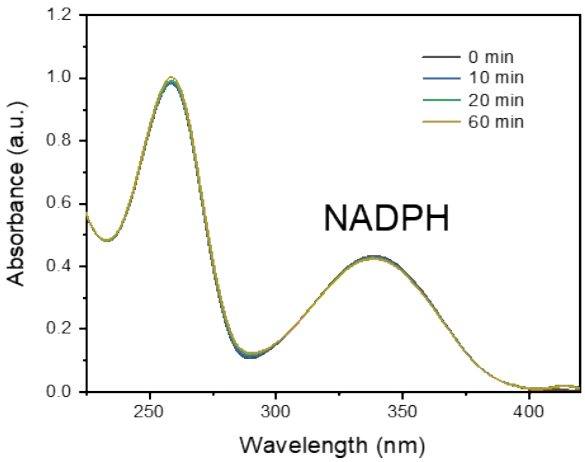

Fig. S12 The UV-vis spectra of NADPH in the air at different times.

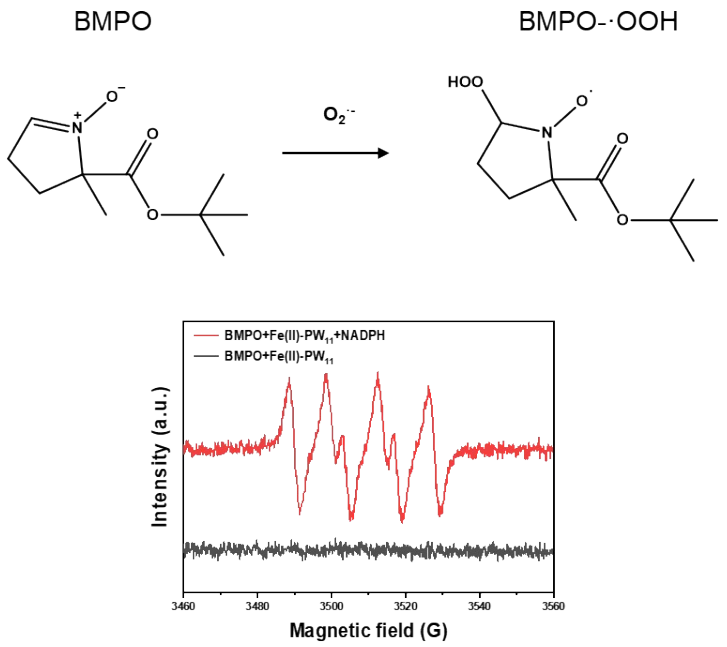

Fig. S13 The EPR spectra for detecting $O_2^{\bullet-}$ using BMPO as a spin-trap agent under air conditions. c(Fe(II)-PW_{11}) = 1 mg/mL, c(BMPO) = 100 mM.

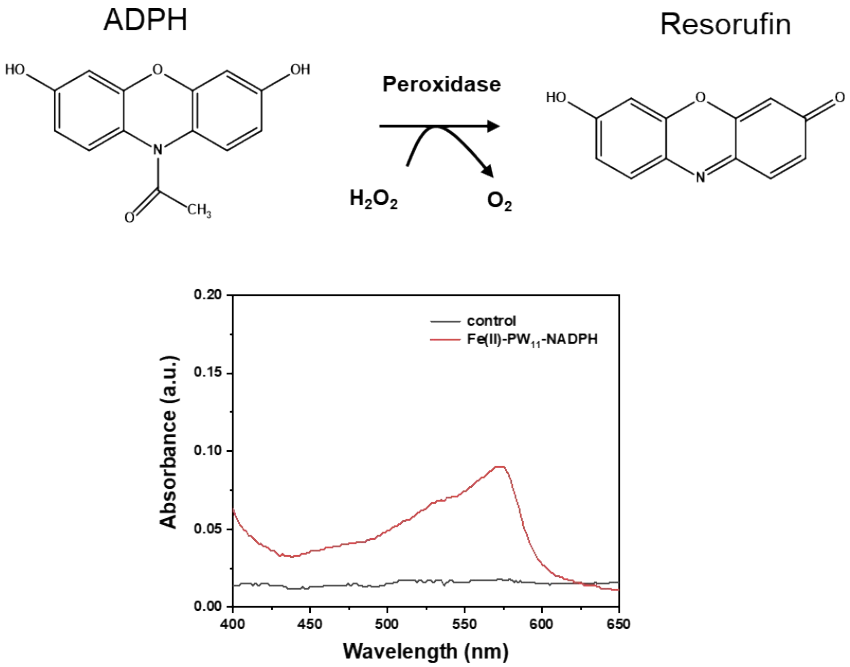

Fig. S14 The UV-vis spectra for detecting H_2O_2 using ADPH as an indicator with the presence of horseradish peroxidase (HPR).

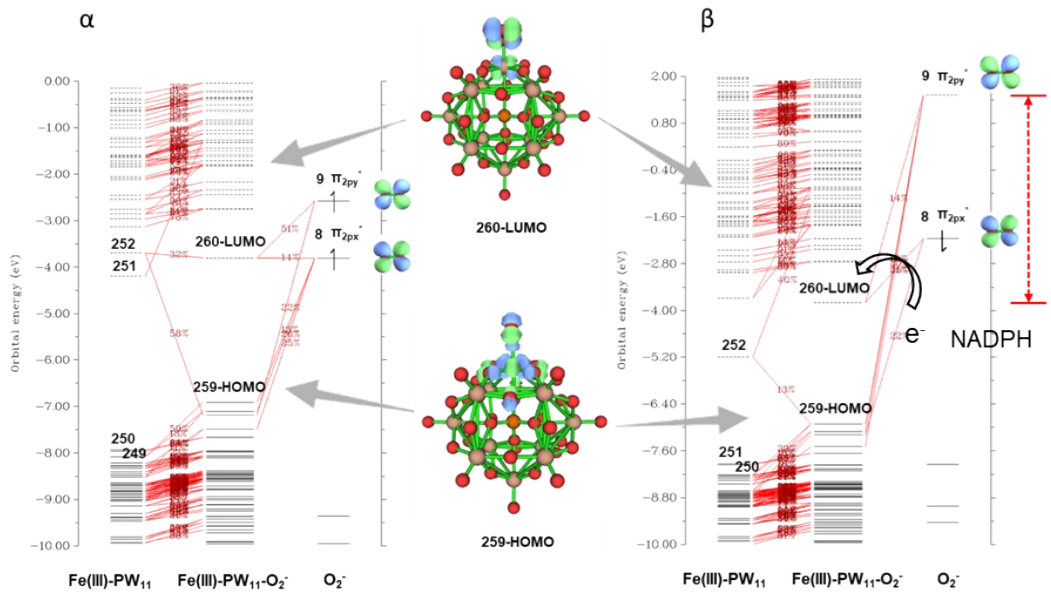

Fig. S15 Calculated orbital interaction diagram for Fe(II)-PW_{11} activated O_2.

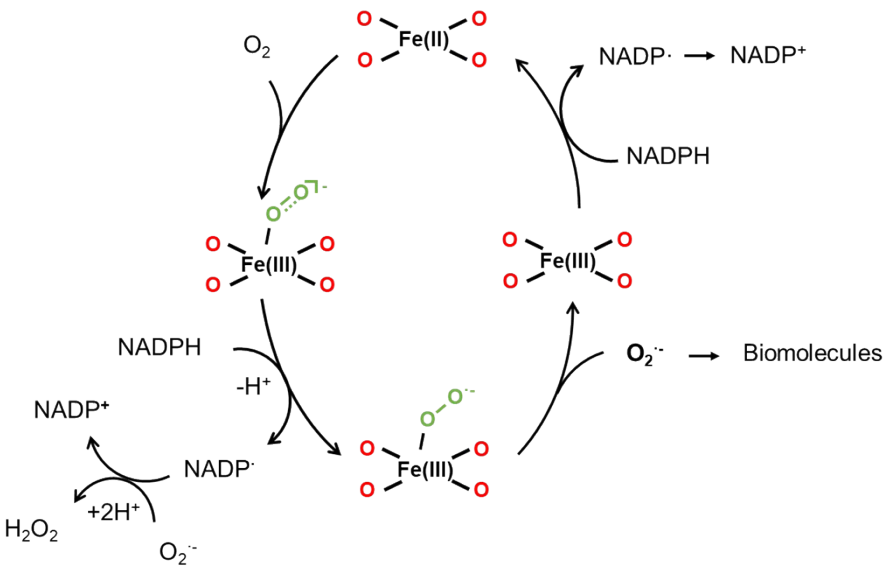

Fig. S16 The mechanism of Fe(II)-PW_{11}-catalyzed NADPH oxidation with NOX-like activity.

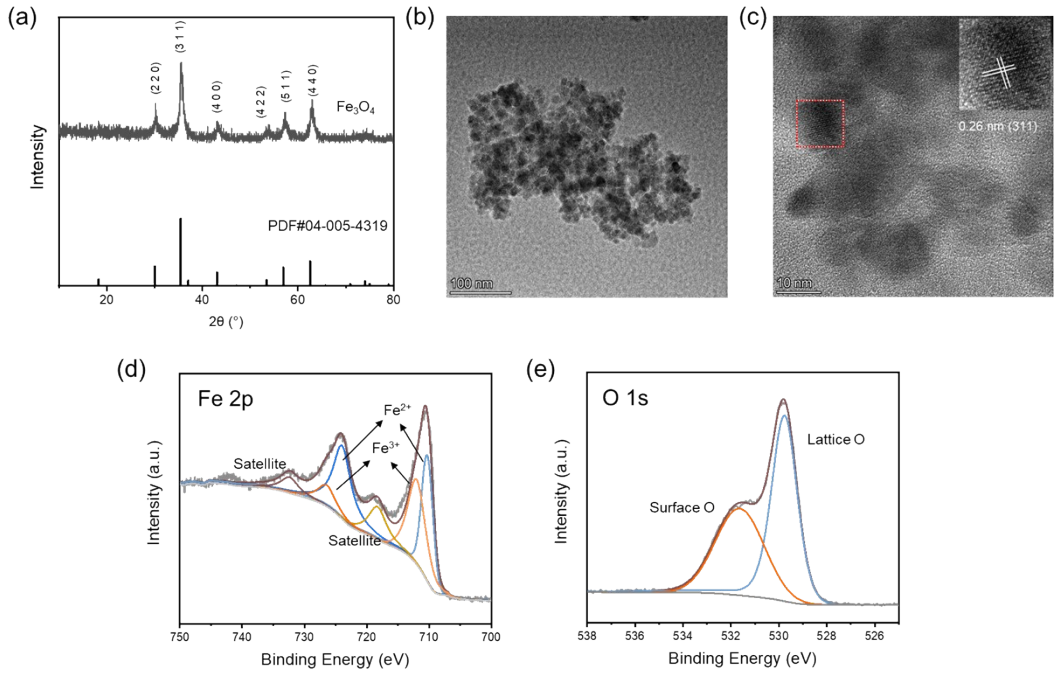

Fig. S17 The characterizations of Fe_3O_4 nanoparticles. (a) XRD pattern. (b) TEM image. (c) HRTEM image. The XPS of (d) Fe 2p and (e) O 1s.

The XRD diffraction peaks of Fe_3O_4 at 30.1°, 35.1°, 43.2°, 53.4°, 56.9° and 62.5° was assigned to the (220), (311), (400), (422), (511) and (440), which confirm its crystal structure (PDF#04-005-4319) (Fig. S17-a). This is in accordance with the uniform irregular morphologies of Fe_3O_4 nanoparticles (TEM characterization in Fig. S17-b), which exhibited the distinct lattice fringe spacings of (311) planes at 0.26 nm (HRTEM characterization in Fig. S17-c). Besides, the elemental valence state of the Fe_3O_4 was characterized by XPS, which confirmed the presence of Fe^{2+} and Fe^{3+} (Fig. S17-d) and recording O 1s signals attributed to the lattice oxygen and surface oxygen species (Fig. S17-e).

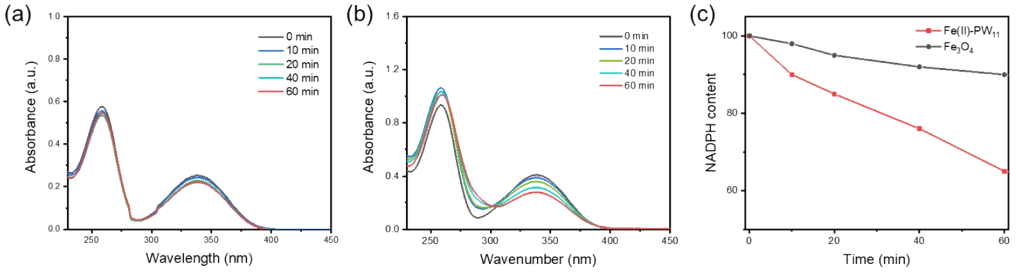

Fig. S18 The NOX-like activity of Fe_3O_4 nanoparticles and Fe(II)-PW_{11}. The UV-vis spectra of NADPH (a) Fe_3O_4 (40 μg/mL with Fe content of 4×10^{-4} mol/L) nanoparticles in air at different times and (b) with Fe(II)-PW_{11} (1 mg/mL with Fe content of 4×10^{-4} mol/L). (c) The NADPH content with the addition of Fe(II)-PW_{11} and Fe_3O_4 nanoparticles.

As demonstrated in Fig. S18, the obvious absorbance of NADPH at 339 nm decreased after adding Fe(II)-PW_{11}, while no significant change of NADPH was observed with Fe_3O_4 nanoparticles added. After 1 h (Fig. S18-c), only 68% of NADPH remained in the Fe(II)-PW_{11} group, much lower than that of the Fe_3O_4 group (90%). This demonstrated that the single-site Fe(II)-PW_{11} showed better catalytic performance than Fe_3O_4.

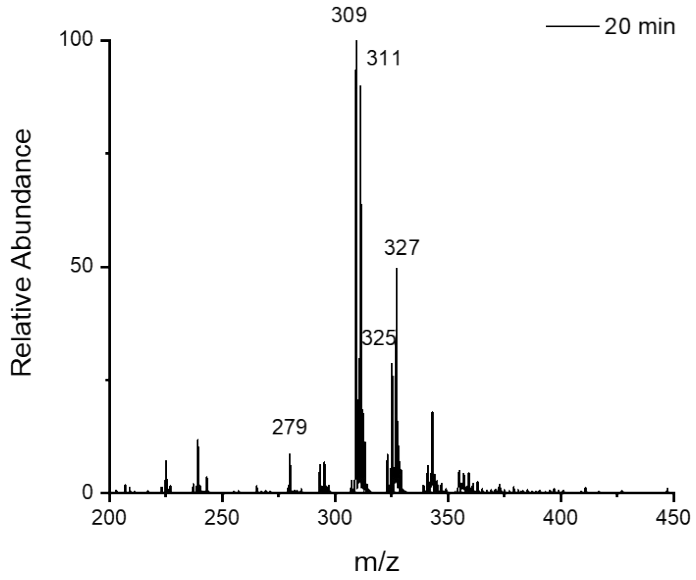

Fig. S19 MS spectra of LA oxidized by Fe(II)-PW_{11} with NADPH at 20 min.

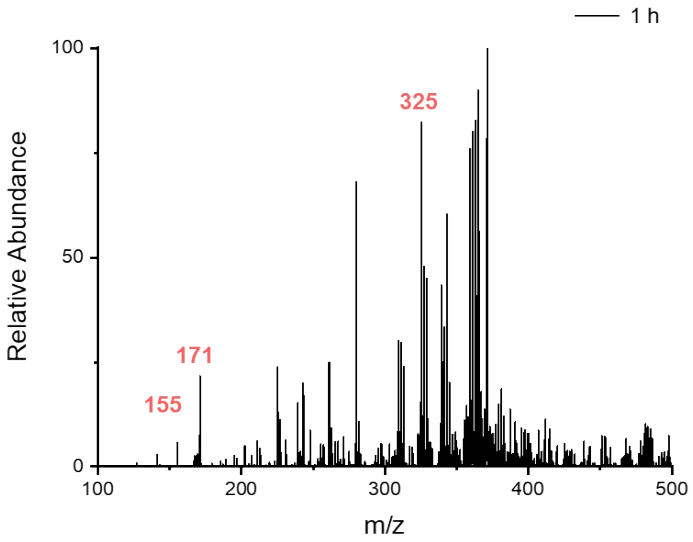

Fig. S20 MS spectra of LA oxidized by Fe(II)-PW_{11} with NADPH at 1 h.

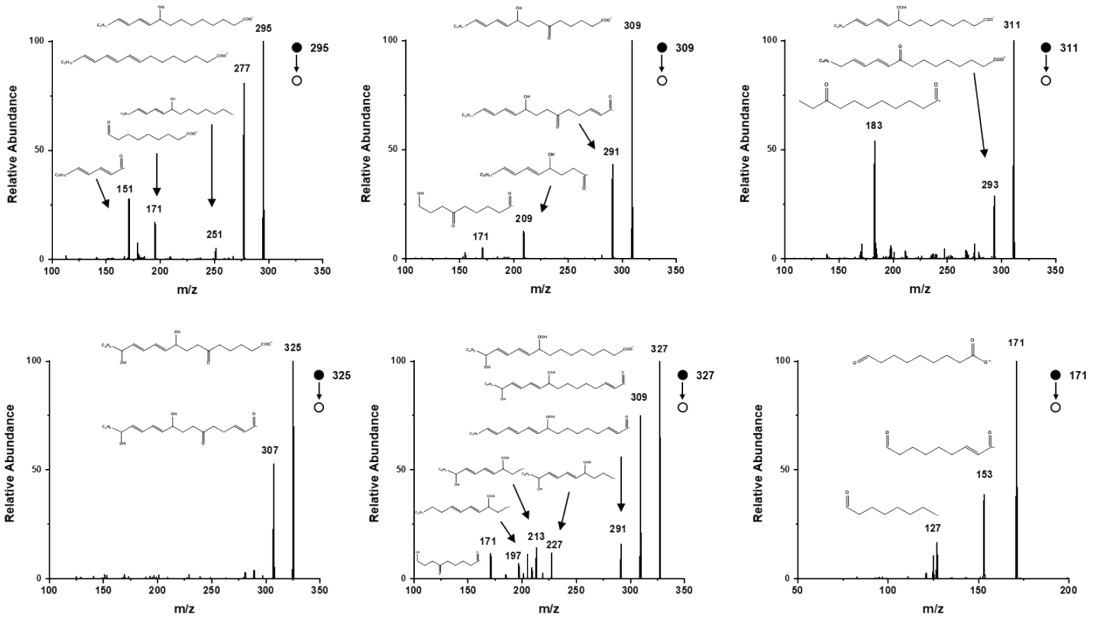

Fig. S21 CID of LA peroxidation intermediates.

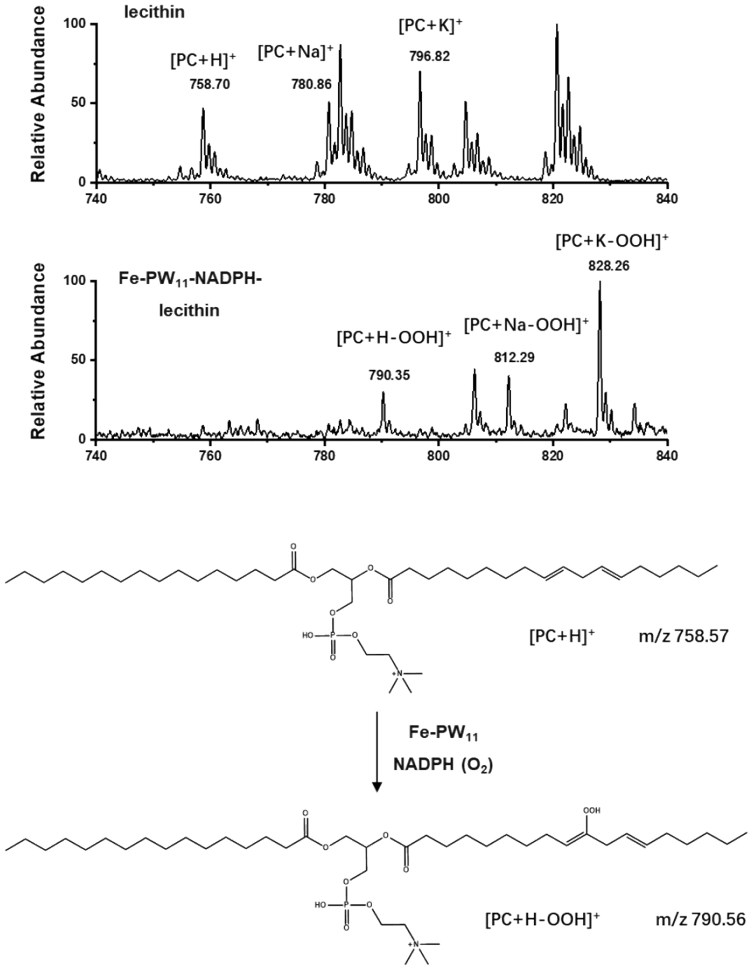

Fig. S22 The MS signal of lecithin with and without Fe(II)-PW_{11} and NADPH.

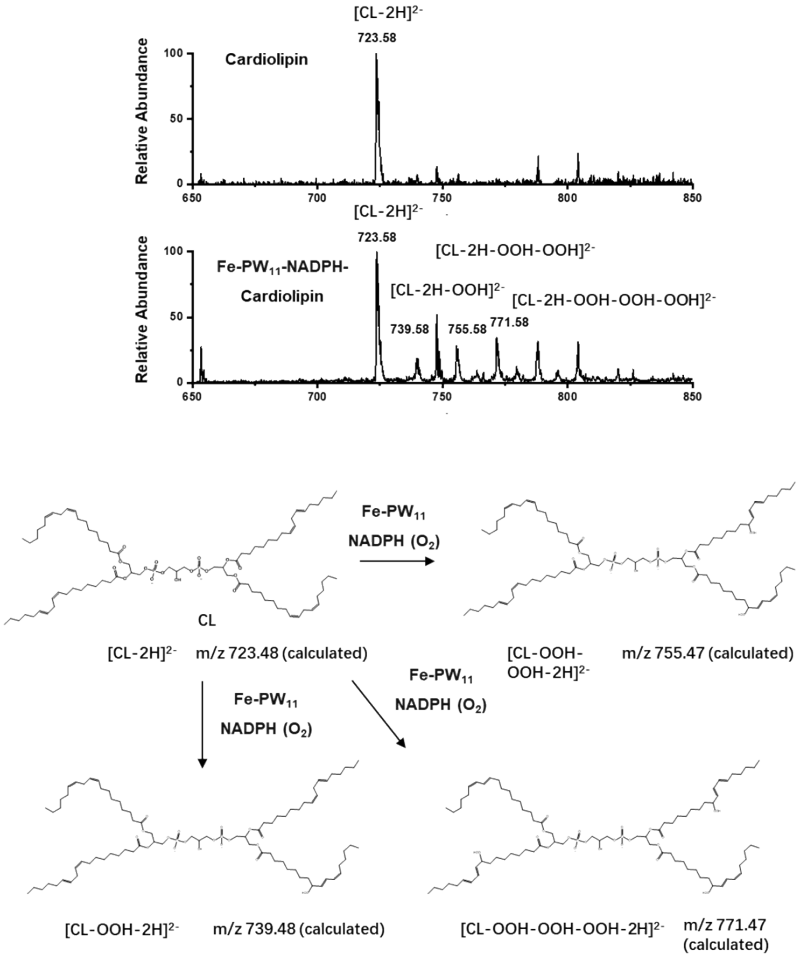

Fig. S23 The MS signal of cardiolipin with and without Fe(II)-PW_{11} and NADPH.

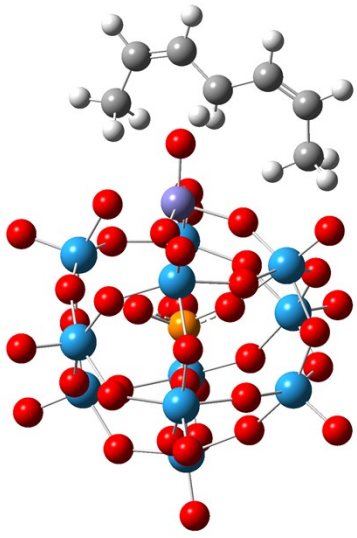

Fig. S24 The TS of the HAT process catalyzed by Fe(IV)=O-PW_{11} with *cis, cis*-1,4-pentadiene as model.

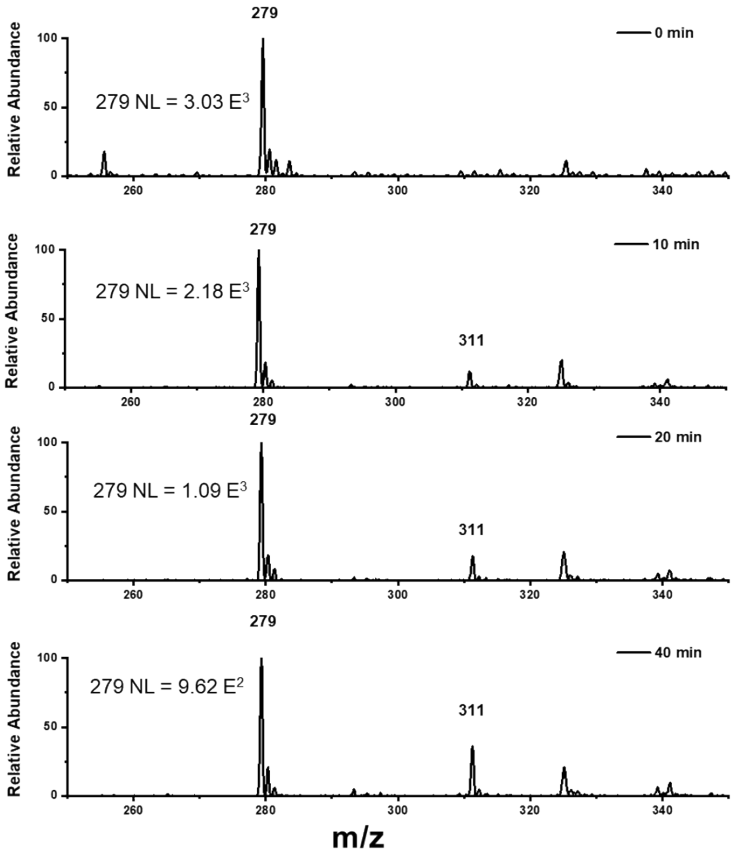

Fig. S25 The LOX-like activity of Fe_3O_4 nanoparticles and Fe(II)-PW_{11}. MS spectra of LA in the Fe_3O_4 nanoparticles system with the addition of NADPH in air at different times.

Treated with Fe(II)-PW_{11} for 20 min, $[LA-H]^-$ at m/z 279 significantly decreased and LA peroxidation products were recorded including $[LA-OH - H]^-$ (at m/z 295), $[LA=O-OH - H]^-$ (m/z 309), $[LA-OOH - H]^-$ (m/z 311), $[LA=O-OH-OH- H]^-$ (m/z 325) and $[LA-OH-OOH - H]^-$ (m/z 327) (Fig. S19). While treated with Fe_3O_4 nanoparticles (Fig. S25), no significant decrease of $[LA-H]^-$ was recorded at 20 min and a relatively low abundance of LA peroxidation products ($[LA-OOH - H]^-$, m/z 311) was recorded even after 1 h of the treatments. Therefore, the single-site catalyst of Fe(II)-PW_{11} exhibits outstanding catalytic performance compared with the conventional nanoparticles.

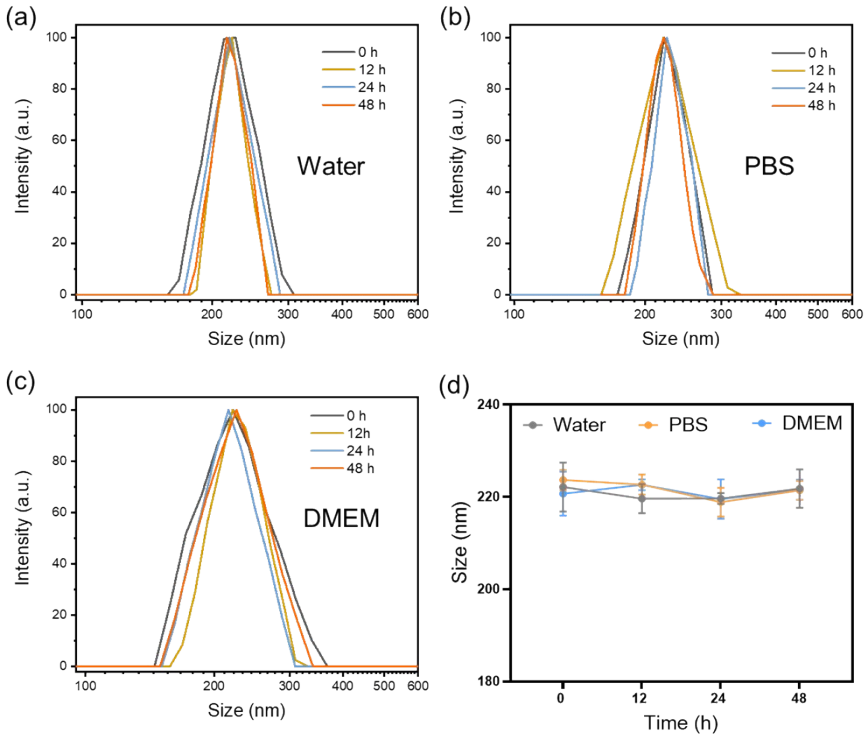

Figure S26 The hydrodynamic size distributions of A-MIL-101@PW_{12} in (a) water, (b) PBS (pH=7.4) and (c) DMEM cell culture medium at different times. (d) The mean size of A-MIL-101@PW_{12} based on (a), (b) and (c) at 0 h, 12 h, 24 h and 48 h.

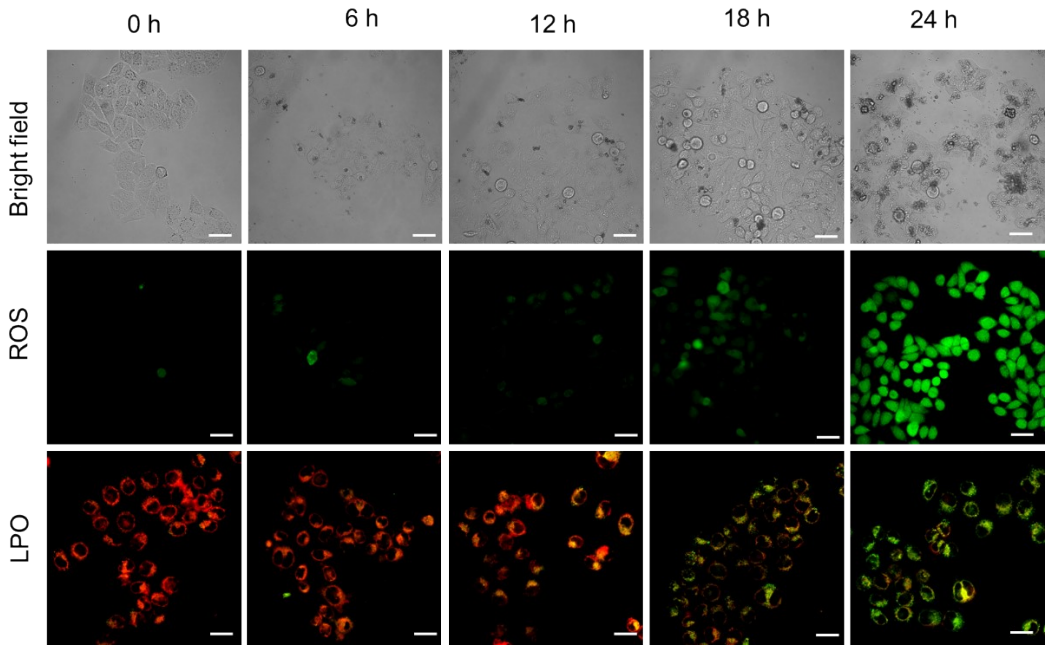

Fig. S27 The cell imaging to evaluate ROS generation and the LPO process in HeLa cells treated with A-MIL-101@PW_{12} at different times. The scan bar is 40 μm.

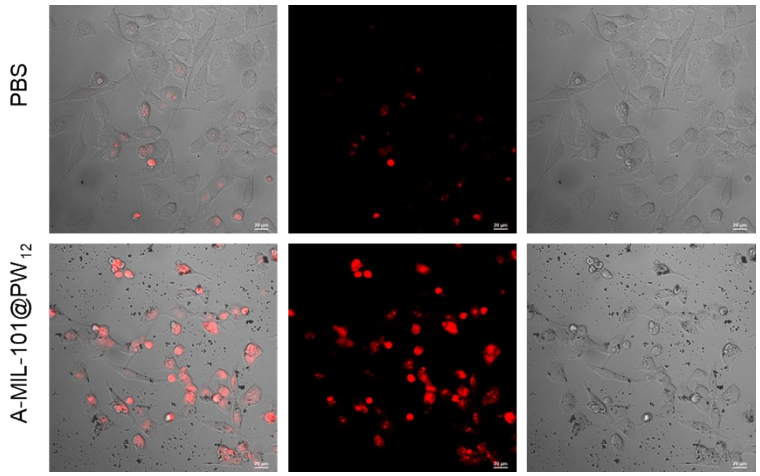

Fig. S28 The intracellular $O_2^{\bullet-}$ detection in HeLa cells.

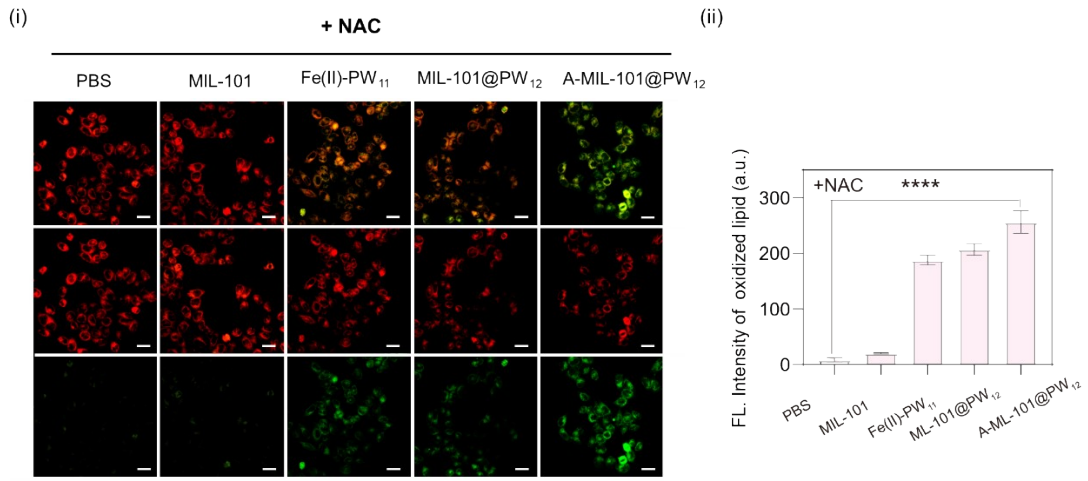

Fig. S29 The LPO verification in HeLa cells (i) Cell imaging treated by different groups with the addition of NAC. (ii) The quantitative statistics of green fluorescence intensity of (i). The scan bar is 40 μm.

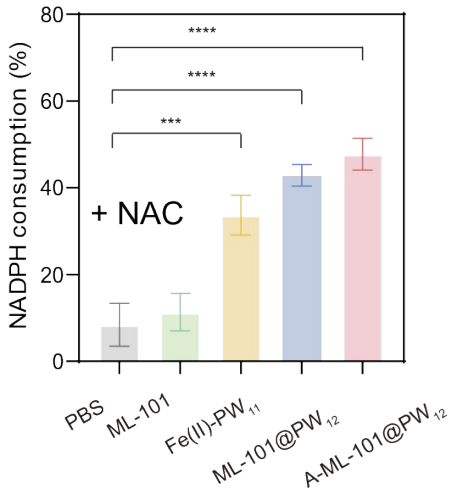

Fig. S30 NADPH consumption of HeLa cells after treated with different groups with the addition of NAC.

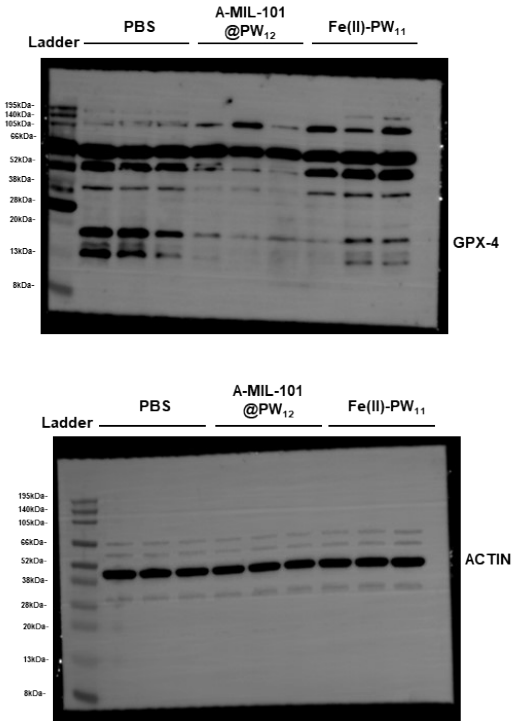

Fig. S31 Western blotting assay of the GPX4 protein levels in cancer cells treated with PBS, Fe(II)-PW_{11} and A-MIL-101@PW_{12}.The experiment was repeated three times independently with similar results.

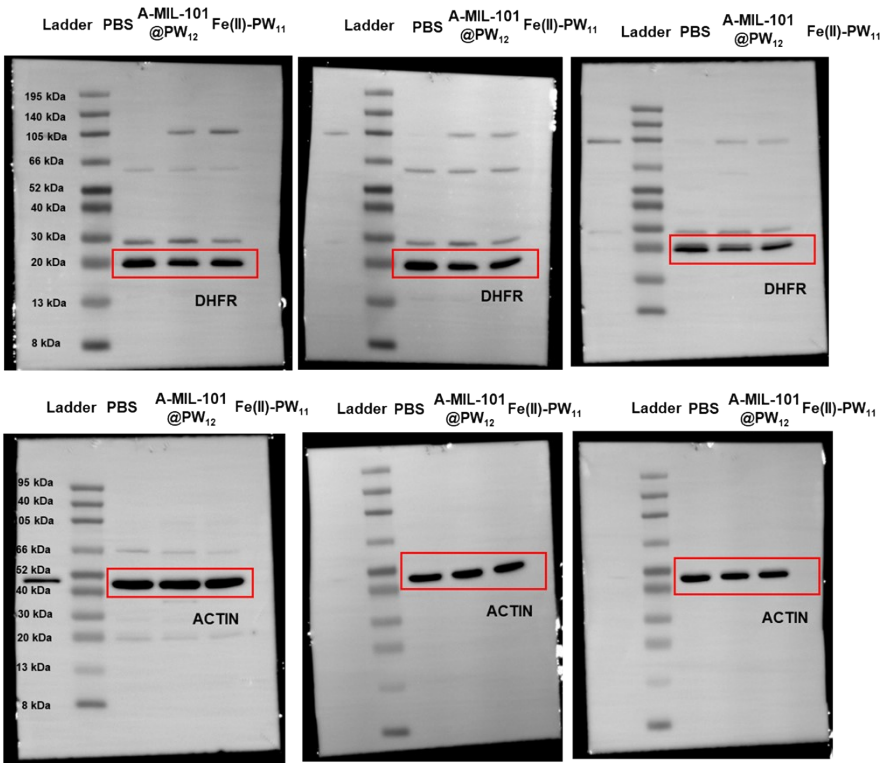

Fig. S32 Western blotting assay of the DHFR protein levels in cancer cells treated with PBS, Fe(II)-PW_{11} and A-MIL-101@PW_{12}.The experiment was repeated three times independently with similar results.

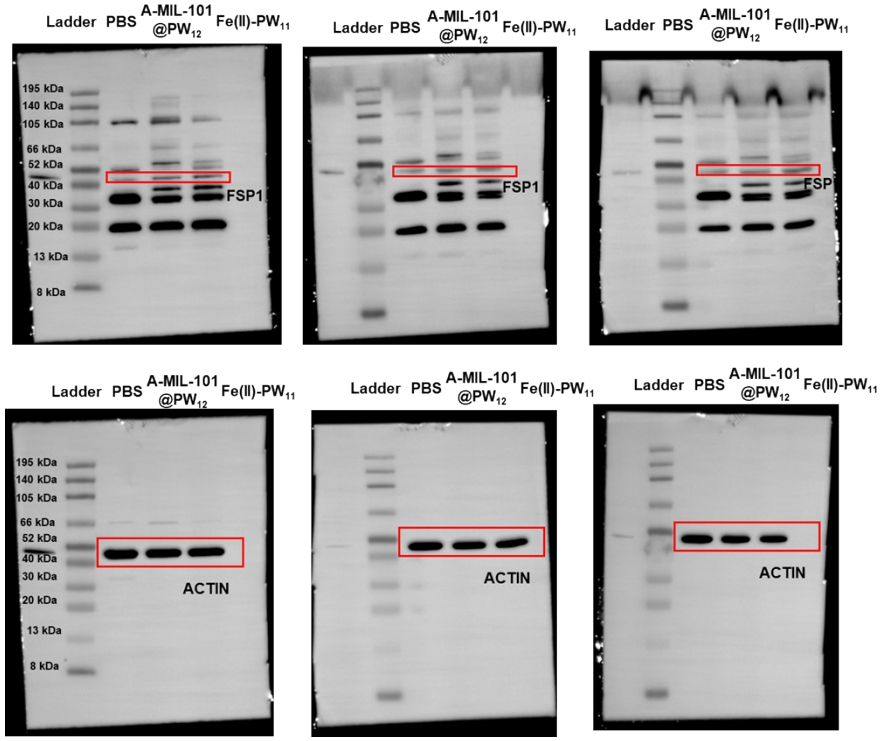

Fig. S33 Western blotting assay of the FSP1 protein levels in cancer cells treated with PBS, Fe(II)-PW_{11} and A-MIL-101@PW_{12}.The experiment was repeated three times independently with similar results.

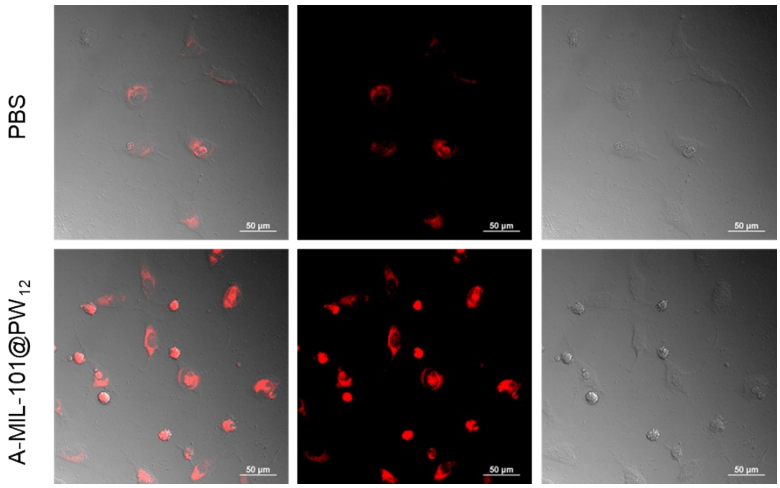

Fig. S34 The Fe^{2+} detection in HeLa cells.

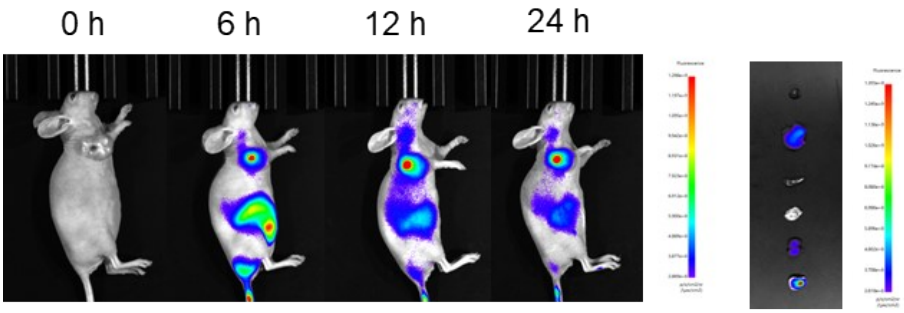

Fig. S35 In vivo fluorescence imaging of HeLa-bearing mice model after intravenous injection of A-MIL-101@PW_{12} at different times and Ex vivo fluorescence imaging of tumor tissues and main organs (heart, liver, spleen, lung and kidney) resected from the mice after 12 h treatment.

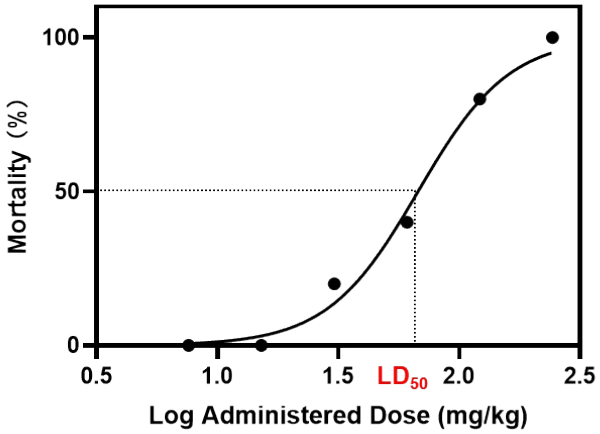

Fig. S36 Dose-response curves of A-MIL-101@PW_{12} in mice (R^2=0.98). Dashed vertical lines indicate LD_{50} values with 67.59 mg/kg (95% fiducial limits: 56.37-80.71).

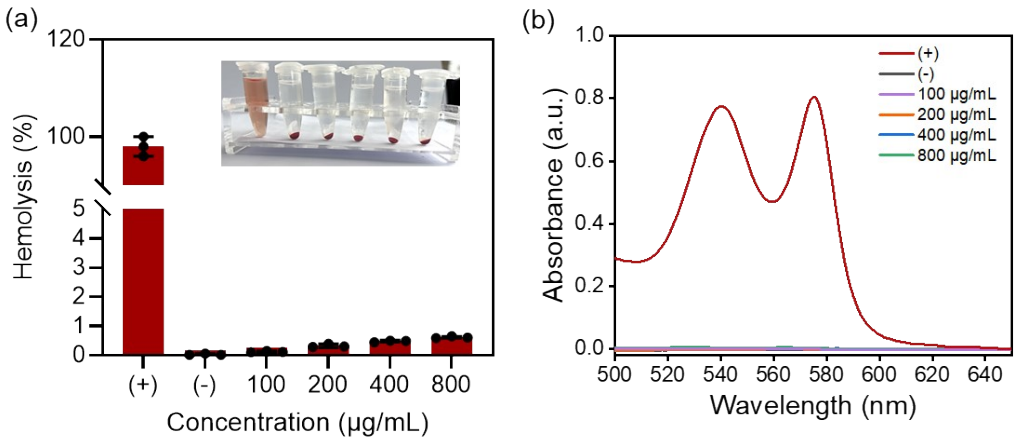

Fig. S37 (a) Hemolysis rate of blood with adding different concentrations of A-MIL-101@PW_{12}. The data were calculated based on the absorbance of the released heme upon hemolysis at 541 nm. The inset is the corresponding image of different samples. Data are presented as mean ± s.d. (n = 3). (b) The absorbance of the supernatants.

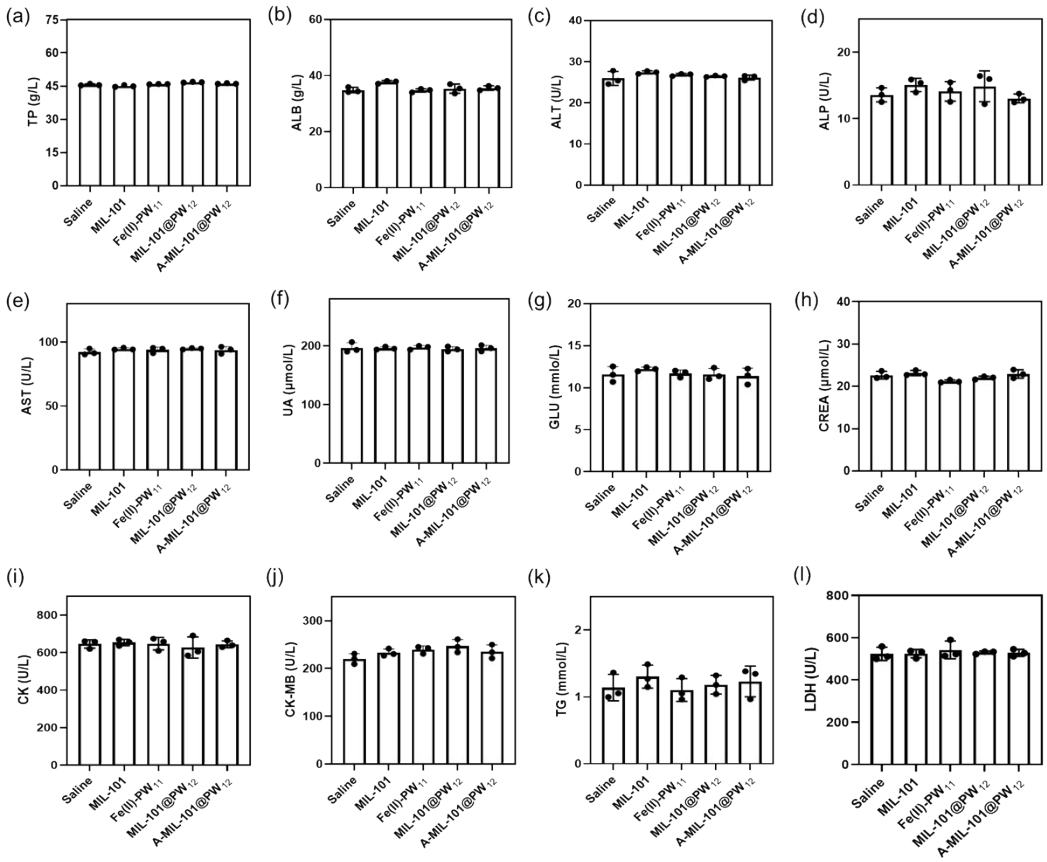

Fig. S38 Serum biochemical analysis of mice with different treatments. (a) Total protein (TP). (b) Albumin (ALB). (c) Alanine aminotransferase (ALT). (d) Alkaline phosphatase (ALP). (e) Aspartate aminotransferase (AST). (f) Uric acid

(UA). (g) Glucose (GLU). (h) Creatinine (CREA). (i) Creatine kinase (CK). (j) Creatine kinase MB (CK-MB). (k) Triglyceride (TG). (l) Lactate dehydrogenase (LDH). Data are presented as mean±s.d. (n=3).

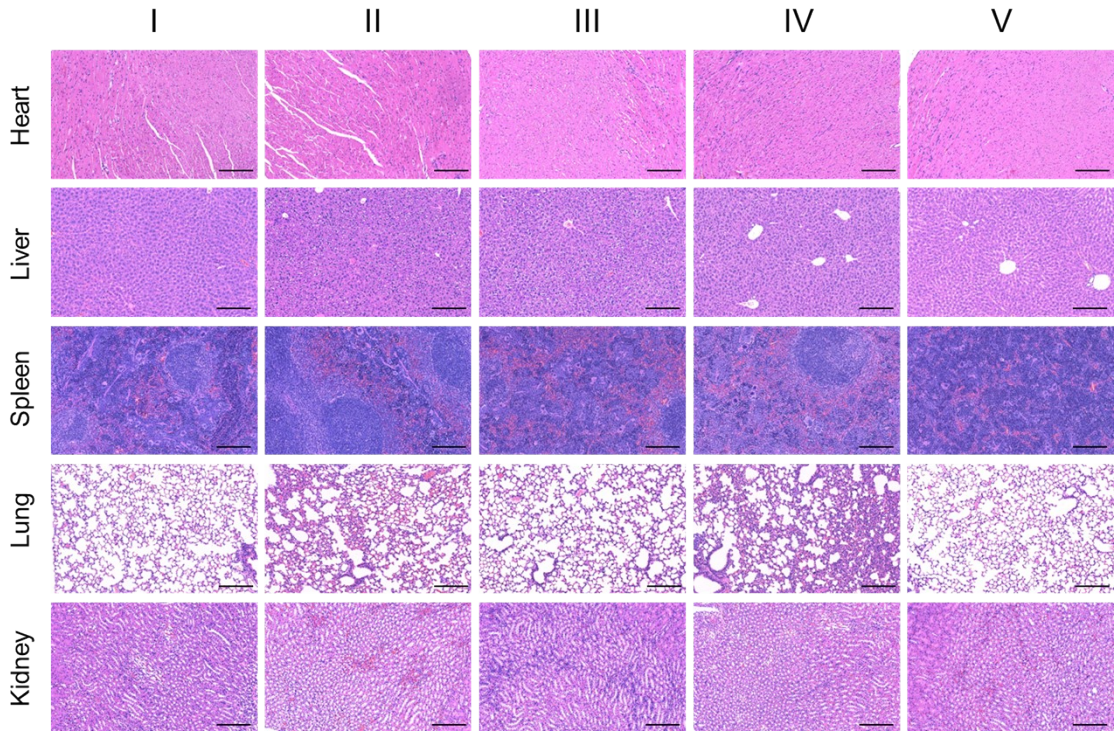

Fig. S39 H&E-stained images of major organs of mice after treated with different nanomedicines. The scale bar is 200 μm.

Reference

1. M.J. Frisch, Gaussian 09, 2009, Revision D.01. M. J. Frisch, G. W. Trucks, H. B. Schlegel, G. E. Scuseria, M. A. Robb, J. R. Cheeseman, G. Scalmani, V. Barone, B. Mennucci, G. A. Petersson, H. Nakatsuji, M. Caricato, X. Li, H. P. Hratchian, A. F. Izmaylov, J. Bloino, G. Zheng, J. L. Sonnenberg, M. Hada, M. Ehara, K. Toyota, R. Fukuda, J. Hasegawa, M. Ishida, T. Nakajima, Y. Honda, O. Kitao, H. Nakai, T. Vreven, J. A. Montgomery, J. E. Peralta, F. Ogliaro, M. Bearpark, J. J. Heyd, E. Brothers, K. N. Kudin, V. N. Staroverov, R. Kobayashi, J. Normand, K. Raghavachari, A. Rendell, J. C. Burant, S. S. Iyengar, J. Tomasi, M. Cossi, N. Rega, J. M. Millam, M. Klene, J. E. Knox, J. B. Cross, V. Bakken, C. Adamo, J. Jaramillo, R. Gomperts, R. E. Stratmann, O. Yazyev, A. J. Austin, R. Cammi, C. Pomelli, J. W. Ochterski, R. L. Martin, K. Morokuma, V. G. Zakrzewski, G. A. Voth, P. Salvador, J. J. Dannenberg, S. Dapprich, A. D. Daniels, Farkas, J. B. Foresman, J. V Ortiz, J. Cioslowski and D. J. Fox, Gaussian 09, Revision D.01, Gaussian Inc.; Wallingford, CT, **2013**.
2. Lu, T., Chen, F. Multiwfn: A multifunctional wavefunction analyzer. *J. Comput. Chem.* 2012, **33**, 580-592.

3. Humphrey, W., Dalke, A., Schulten, K. VMD: Visual molecular dynamics. *J. Mol. Graph. Model.* 1996, **14**, 33-38.